MULTIAXIAL LOW CYCLE FATIGUE BEHAVIOUR OF A MILD STEEL

V. Doquet and A. Pineau
Centre des Matériaux - Ecole des Mines
B.P.87 - 91003 Evry Cédex (France)
UA CNRS N°866

Third International Conference on Biaxial/Multiaxial Fatigue
April 3-6, 1989, Stuttgart, F.R.G.

ABSTRACT

Combined tension and torsion tests were performed on thin tubular specimens of mild steel. These tests were carried out at different values of the ratio, λ between the tensile stress, σ, and the shear stress, τ, ($\lambda = 0; \simeq 0.50; \infty$). For $\lambda \simeq 0.50$ both in-phase and out-of-phase loadings were applied. The fatigue lives varied from 5.10^2 to 10^6 cycles. Optical and scanning electron microscopy were used to analyze the failure modes.

It is shown that the material exhibits either cyclic softening or hardening, depending on the applied strain amplitude and the phase angle, φ between σ and τ. The intersection of the cyclic stress-strain curve with the monotonic tensile curve is shifted towards a lower strain amplitude by out-of-phase loading, compared to uniaxial tests. For a given equivalent strain amplitude the endurance is slightly reduced by non-proportional loading compared to either uniaxial or proportional loading. The fatigue lives correlate better with the equivalent stress amplitudes associated with the various loading conditions. Intergranular crack initiation is promoted by multiaxial, especially out-of-phase, loading. It is shown that the orientation of the transgranular micro-cracks ($\simeq 50$ µm) corresponds to the planes bearing the largest shear strain amplitude. On the other hand the orientation of the major crack (several nomm length) cannot be so easily predicted.

INTRODUCTION

Multiaxial low cycle fatigue is a rather recent research topic but strongly developing since the beginning of the eighties, as shown by the first two international conferences dealing with this subject [1,2] . A large number of studies have now been devoted to FCC materials, especially austenitic stainless steels, while ferritic materials have not been investigated so thoroughly, except three investigations on low alloy ferritic steels [3,4,5]. However it is believed that the comparison of the multiaxial behaviour of materials with different crystallographic structures might well prove to be very fruitful for the understanding of both hardening and damage processes in each kind of material.

As far as cyclic behaviour is concerned, a number of authors have shown a dramatic increase in hardening rates when the materials are submitted to out-of-phase multiaxial fatigue (see eg.[6]. This conclusion was reached in austenitic stainless steels for which an additional hardening as large as 100%, compared to uniaxial cyclic behaviour was observed when the loading ratio λ between the torsional shear stress amplitude and the tensile stress amplitude, $\Delta\sigma$ was close to 0.5. The explanation usually proposed to account for this situation is based upon the interaction of the numerous slip systems activated because of the rotation of principal axis under non-proportional loading. On the other hand proportional multiaxial loading seems to have much less influence on the cyclic behaviour. Again these conclusions are essentially based on the data obtained on FCC materials. In BCC materials, the anomalous hardening associated with non-proportional multiaxial loading appears to be less pronounced, since Brown and Miller [3] reported an effect of less than 14% in a 1% Cr steel, while Sonsino and Grubisic [4] observed an effect of about 40% in a Cr-Mo-Ni steel. It is clear that this research topic deserves more attention. This is one of the reasons why in the present study an attempt is made to investigate this phenomenon in a largely used material, i.e. mild steel.

As far as the fatigue life is concerned it is usually observed that the most damaging loading is that corresponding to 90 degrees out-of phase multiaxial low cycle fatigue. Typically, but again in austenitic stainless steel, it is observed that the fatigue life may be reduced by a factor as large as 10 (see eg. [6]). A large number of correlations between the loading mechanical parameters and the endurance have been proposed. However for a large number of investigators it is now clear that the only promising way of tackling the problem of life prediction is to take into account the directional aspect of fatigue damage instead of fitting endurance curves with any kind of equivalent loading parameter. For example in a 1% Cr-Mo-V steel, Kanazawa et al [7] clearly showed that crack initiation took place along directions undergoing the largest shear strain amplitude and, among these, especially those which were subjected to the largest normal deformation amplitude. However this conclusion, as most of the studies dealing with multiaxial low cycle fatigue, was obtained from a two-dimensional analysis. In the literature dealing with the directional aspect of fatigue crack initiation sites there are very few results which have been reported. However a study devoted to three FCC materials, i.e. an austenitic stainless steel, Alloy 800 and a nickel base superalloy showed, from 3-dimensional observations that tension-compression tests give rise to type A as well as type B microcracks with a little more of the latter type. [8,9] . Here the terminology of type A and B microcracks is that introduced by Brown and Miller [10] . On the other hand, in these three austenitic materials type A microcracks were found to be largely predominant under torsional loading. Here again, it is clear that this problem deserves more attention, especially in the case of ferritic materials.

The aims of the present study were : (i) to contribute to the understanding of the cyclic behaviour of a ferritic steel under multiaxial

low cycle fatigue. Unlike in an other study devoted to 316L stainless steel also presented in this conference [11], the analysis of the cyclic behaviour remains macroscopic since the microscopic-macroscopic approach is up to now only developed for FCC materials; (ii) to discuss the influence of multiaxial loading on the fatigue damage mechanisms; and (iii) to correlate the orientation of microcracks and major cracks with the mechanical loading parameters.

MATERIAL AND EXPERIMENTAL PROCEDURES

The material investigated is a mild steel. The chemical composition and the mechanical properties are given in Table 1 and 2 respectively. An annealing treatment was applied at 1000°C during half an hour under argon, followed by furnace cooling. This produced an homogeneous microstructure made of ferritic grains - 30 μm average size - with 3% residual pearlite. Tubular specimens (Fig.1) were mechanically polished and then electropolished. The first tests were run under displacement control but an extensometer was soon designed to measure and control both the longitudinal and the shear deformation amplitudes $\Delta\epsilon$ and $\Delta\gamma$ along the gage length of the specimens. All tests were run at room temperature and the equivalent strain rate was kept approximately of the order of $10^{-3}s^{-1}$ for each one. Failure was defined as a 15% drop in shear or axial stress amplitude.

The uniaxial fatigue behaviour of the material was first characterized under tension-compression (Table 3) and reversed torsion (Table 4). In these tables, the plastic strain amplitudes were measured on the hysteresis loops at zero load. Combined tension and torsion tests were then carried out either in-phase or 90 out-of-phase with loading ratios $\lambda = \frac{\Delta\tau}{\Delta\sigma}$, $\lambda' = \frac{\Delta\gamma}{\Delta\epsilon}$ near 0.5 and $\sqrt{3}$, respectively (Table 5).

Data acquisition was performed by a microcomputer. Further data processing permits the calculation of the Tresca and Von Mises equivalent stress and strain amplitudes. Under out-of-phase loading these amplitudes are calculated as follows. Stress or strain paths are first drawn using Von Mises or Tresca coordinates $\left[\left(\epsilon, \frac{\gamma}{\sqrt{3}}\right), \left(\sigma, \sqrt{3}\tau\right)\right]$ or $\left[\left(\epsilon, \frac{2\gamma}{3}\right), (\sigma, 2\tau)\right]$. The radius of the circumscribing circle is called the "equivalent amplitude". The plastic equivalent amplitudes were defined in the same way by plotting $\left(\epsilon - \frac{\sigma}{E}\right)$ versus $\left(\frac{\gamma}{\sqrt{3}} - \frac{\sqrt{3}\tau}{\mu}\right)$ or $\left(\epsilon - \frac{\sigma}{E}\right)$ versus $\left(\frac{2\gamma}{3} - \frac{2\tau}{\mu}\right)$. All tests were performed under fully reversed conditions - i.e. $R_\epsilon = R_\gamma = -1$ - so that the circumscribing circle is always centered on the origin of the axis.

RESULTS AND DISCUSSION

1) Cyclic behaviour

Under uniaxial fatigue the material exibits either cyclic softening or hardening, depending on the applied strain amplitude (Fig.2) so that the cyclic stress-strain curve crosses the monotonic tensile curve at a point where $\frac{\Delta\epsilon}{2} = 0.3\%$ and $\frac{\Delta\sigma}{2} = 210$ MPa (Fig.3).

Two conflicting effects may be involved to explain this behaviour : (i) Unpinning of dislocations from Cottrell atmospheres which contributes to the increase in mobile dislocations density giving rise to work softening and (ii) Raising of internal stresses due to glide systems interactions leading to usual work hardening.

Figures 4a and B show that Tresca equivalents fit both tension and torsion cyclic stress-strain curves better than Von Mises ones.

Some scatter is observed, especially for the in-phase tension and torsion tests. Note that full lozanges relate to tests 340a, b and c which were performed successively on the same specimen by raising the strain amplitude. Thus the corresponding data are not as reliable as the other ones because of damage accumulation. In spite of this scatter it can be concluded that in-phase loading has no definite effect on the cyclic behaviour of this steel.

On the other hand out-of-phase loading tends to increase the equivalent stress response of the material up to a maximum of 40% additional hardening above the mean uniaxial stress-strain curve. Thus, in our material the effect is of the same order of magnitude as observed by Sonsino and Grubisic [4].

The rotation of principle axis during out-of-phase loading generates more active slip systems than in-phase loading does. This is apparent from the comparison of two specimens submitted to comparable strain amplitudes (Fig. 5a and b). In particular surface rumpling is much pronounced for the specimen subjected to out-of-phase loading. In a companion paper devoted to a stainless steel [11] the multiplicity of slip systems has been quantitifed. In the ferritic material this proved almost impossible because of the very wavy aspect of slip lines observed on the specimens surface. The increase in slip activity enhances the second of the two conflicting effects described earlier. The crossing of the cyclic stress-strain curve with the monotonic tensile one is thus shifted towards $\frac{\Delta\epsilon}{2} = 0.16\%$ by out-of-phase loading, compared to 0.3% for uniaxial tests.

To account for this extra hardening Kanazawa et al.[7] defined a non-proportionality factor F as folows :

$$F = \frac{\text{shear strain range at } 45^\circ \text{ to maximum shear plane}}{\text{maximum shear strain range}}$$

This parameter "measures" the amount of deformation on other planes than those activated under proportional loading. Thus it is null for in-phase loading and reaches its maximum value (=1) for 90° out-of-phase

loading when $\lambda' = \frac{\Delta\gamma}{\Delta\epsilon} = 1+\nu$ where ν is the Poisson's ratio. For intermediate cases, F is given in reference [7]. This definition applies only to type A planes. It is therefore only valid in a two-dimensional analysis. We kept to this pattern and calculated F factor for our tests. The equation :

$$\frac{\sigma_{eq\ Tresca}}{1 + lF} = k \left(\frac{\Delta\epsilon p_{eq\ Tresca}}{2}\right)^n$$

with an adjusted l value of 0.31 proved efficient to describe the behaviour of our steel (Fig.5). This value of l is larger than that found in 1% Cr-Mo-V steel [3]. This reflects the greater sensitivity of mild steel to the effect of non-proportional loading.

2) Damage and fatigue

Although we do not rely necessarily on equivalent based correlations, these equivalents are convenient for presenting results. The life-times of the specimens are drawn as a function of the applied equivalent plastic strain amplitude in Figure 7.

2a) Tension and torsion endurance

The first striking feature is that for equivalent strain amplitudes - according to Von Mises as well as to Tresca criteria - the endurance under reversed torsion is up to four times larger than that under tension-compression. A compiling of data from the literature [4, 8, 12,13] shows that this is a rather general rule which is even more pronounced for austenitic materials of widely different mechanical properties (Fig.8).

Sequential and interrupted tests showed that this difference in endurance might arise from a longer propagation stage under torsion than under tension whereas the initiation stage in both cases would be expressed by the same law [8, 9]. To support this idea one might say that for equivalent strain amplitudes - e.g. according to Von Mises - the planes undergoing either the largest plastic shear amplitude or the largest normal strain amplitude bear respectively :

For tension :
$$\begin{cases} \Delta\gamma_p^{Max} = 2\left(\frac{\Delta\epsilon p_{eq}}{2}\right)(1+\nu) = 3\left(\frac{\Delta\epsilon p_{eq}}{2}\right) \\ \Delta\epsilon_{n,p}^{Max} = 2\left(\frac{\Delta\epsilon p_{eq}}{2}\right) \end{cases}$$

For torsion :
$$\begin{cases} \Delta\gamma_p^{Max} = 2\left(\frac{\Delta\gamma p_{nominal}}{2}\right) = 2\sqrt{3}\left(\frac{\Delta\epsilon p_{eq}}{2}\right) = 3.46\left(\frac{\Delta\epsilon p_{eq}}{2}\right) \\ \Delta\epsilon_{n,p}^{Max} = \left(\frac{\Delta\gamma p_{nominal}}{2}\right) = \sqrt{3}\left(\frac{\Delta\epsilon p_{eq}}{2}\right) = 1.73\left(\frac{\Delta\epsilon p_{eq}}{2}\right) \end{cases}$$

So, for equivalent strain amplitudes :

$$\begin{cases} \Delta\gamma_{p,max}^{Tension} < \Delta\gamma_{p,max}^{Torsion} \\ \Delta\epsilon_{n,Max}^{Tension} > \Delta\epsilon_{n,Max}^{Torsion} \end{cases}$$

In the literature there is a body of growing consensus to associate each of these parameters to one part of the fatigue life [5-9]. $\Delta\gamma_p$ is closely related to the crack initiation stage of duration N_a, while mode I crack propagation is governed by $\Delta\epsilon_n$. Therefore a natural conclusion would be that :

$$\left(\frac{N_a}{N_f}\right)^{Tension} > \left(\frac{N_a}{N_f}\right)^{Torsion}$$

The fact that the divergence between tension and torsion endurance curves increases for small strain amplitudes, i.e. for life-times essentially spent in propagation stage, is somewhat contradictory to these ideas. Moreover Smith and Pascoe [14] and Brown and Miller [15] found an accelerating influence of the second principal stress that exists under torsion ($\sigma_{II} = -\tau$) and not under tension ($\sigma_{II} = 0$) on the propagation of a mode I crack.

Finally it is not impossible that the difference between tension and torsion is related to the experimental way of defining failure. At large plastic strain, part-through torsion cracks are prone to propagate under an apparent mode II or mode III. This results in tremendously large crack closure effect as shown by a number of authors, see e.g. [16,19]. A torsional crack is then still able to bear a significant torque. Even if the major crack propagates under mode I, its inclination (=45°) from the bearing surface makes its propagation less "efficient" to decrease the load bearing capacity than that of a crack under tension that lies in the bearing plane.

2b) Multiaxial fatigue life

Figures 7a and b show that for a given equivalent strain amplitude multiaxial proportional loading does not affect endurance whereas out-of-phase loading divides it by a factor of 2, compared to tension results.

If the life-times are now plotted versus equivalent stress amplitudes (Fig.9) the damaging effect of non-proportional loading is less apparent, because it is partly related to additional hardening. An equivalent stress definition intermediate between Von Mises's and Tresca's ones - i.e. $\sigma_{eq} = \sqrt{\sigma^2 + (k\tau)^2}$ with $\sqrt{3} < k < 2$ - would fit all our data.

An other way of correlating the results is provided by Socie's representation [6], somewhat modified : $\frac{\gamma_{max}}{2} + \frac{\Delta\epsilon_n}{2}$ versus N_f (Fig.9c). The modification lies in the $\frac{1}{2}$ coefficient affected to γ_{max} and in a three dimensional calculation of the mechanical loading parameters [18].

2c) Microstructural damage

S.E.M. observations of specimens outer surfaces showed that large strain amplitude and non-proportionality promote inter-granular crack initiation. The rate of intergranular cracking - defined as the ratio of the sumed lengths of intergranular microcracks to the sumed lengths of all cracks observed - was measured in several cases (Table 5). For highly non-proportional loading, intergranular crack initiation is predominant. Parsons and Pascoe [5]observed a similar phenomenon on both a ferritic and austenitic material.

This seems rather surprising for two reasons. First in B.C.C. materials numerous dislocation glide possibilities should accommodate deformation incompatibilities between adjacent grains. Second, out-of-phase loadings under which each plane successively undergoes shear stresses have a tendency to produce more homogenous deformation from one grain to another. An explanation may be based upon the notion of local irreversibility. For each type of applied loading there exist components of deformation - either normal or shear - perpendicular to the free surface of specimens. The load being fully reversed, these alternating components should not induce any surface rumpling. Surface distorsion is thus a manifestation of the local irreversibility of dislocation glide. Figure 5 strongly suggests that, because of higher internal stresses and rotation of principle axis non-proportional loading increases local irreversibility.

The directional aspect of microstructural damage.

The orientations of intergranular microcracks were measured. No significant relation with any kind of mechanical loading parameter was found.

Trans-granular crack initiation observations on both the free surface and a longitudinal cut of specimens were performed. Histograms showing the angular repartition of damage around the direction of the specimens axis were obtained (Fig.10).

For tension tests the histograms (Fig.10a) show that both type A and B cracks are present. For torsion tests (Fig.10b) only type A cracks are observed in a longitudinal cut but a small amount of other cracks is present on the free surface of the specimen. These observations are in agreement with those carried out on austenitic materials [8,9].

For in-phase loading a 3D calculation of the directions of planes bearing the largest amplitude of shear strain was performed [18].This calculation predicts that these planes intersect the outer surface with an inclination of either 20° or -70° to the specimen axis and intersect the longidudinal cut with an inclination comprised between 36° and 90°. The observations confirm this prediction rather well (Fig.10c).

Eventually for one of the out-of-phase tests the 3D calculation of planes undergoing the largest - to within 5% - amplitude of shear strain predicts surface inclination of either [0 to 15°] or [-76 to -90°] with sign exception and an inclination into the depth from 76° to 90°. The observations are in agreement with these predictions (Fig.10d).

The conclusion is not new : transgranular cracking is essentially governed by the shear strain amplitude undergone by each plane.

2d) Main crack propagation direction

Many authors have already underlined the transition occurring for several materials above a given amplitude of deformation in the propagation mode under reversed torsion see e.g. [5,16]. Figure 11a illustrates this phenomenon. At low strain amplitude a mode I helicoïdal crack develops at 45° the axis of the tube whereas at higher strain amplitude the main crack is either longitudinal or transversal.

In a detailed study Sakane et al. [21]attempted to show that the latter kind of cracks grow by coalescence of the numerous shear microcracks left by the initiation stage . It is felt that plasticity-induced crack closure effects might contribute to account for this transition.

In Figure 11b the direction of the main crack in a specimen subjected to in-phase tension and torsion is compared with the direction of first principal axis. Instead of developping at 60° to the axis of the tube the crack mainly propagates with an inclination of approximately 80°.

For the out-of-phase loading 3D calculations of planes undergoing the largest amplitude - to within 5% - of opening stress predicts for test 232 a surface crack inclination from 66° to 90° and for test 252 an even broader range of inclination : from 50° to 90°. These "uncertainties" do not arise from calculation lack for accuracy but from the homogeneity of the opening stress amplitude for such loading ratios λ. However the observations show that even if one part of each crack follows the calculated direction most of their extension takes place along planes inclined by 30° to 45° to the axis of the specimens (Fig.11c).

Moreover, the roughness of fracture surfaces, in addition to the branched aspect of cracks and the fact that each part of the crack undergoes mixed mode loading with a phase angle depending on its orientation suggest that crack closure effects must have a drastic importance under out of phase loading. Therefore, the damaging character of non-proportional loading might lie rather in a shortened crack initiation period than in an accelerated propagation stage.

CONCLUSIONS

(1) Cyclic softening or hardening observed under uniaxial cycling, depending on the applied strain amplitude is related to the competition between the formation of fresh dislocations unpinned from Cottrell atmospheres and the increase in internal stresses due to the interactions between glide systems.

(2) The increase in slip activaty due to the rotation of principal axis during out-of-phase loading promotes the cyclic hardening component. For an equivalent Von Mises strain amplitude of 0.5%, 90° out-of-phase loading gives rise to an increase of the cyclic stress-strain curve by about 40%, compared to the uniaxial tension-compression tests. In-phase

tension-torsion loading leads to no significant effect on the cyclic tress-strain behaviour.

(3) It is possible to describe empirically this cyclic behaviour by using a non-proportionality factor, F, which is the ratio between the shear strain range at 45° to maximum shear plane and the maximum shear strain range to fit the resutls.

(4) The fatigue lives measured under pure reversed torsion are larger than those under tension-compression loading, by a factor of about 5, depending on the applied strain amplitude. It is suggested that this difference might be related to the life spent in crack propagation instead of the life corresponding to crack initiation and to the experimental way of defining fatigue failure.

(5) Out-of-phase loading shortens the endurance compared to uniaxial or in-phase loading when the fatigue lives are analyzed in terms of equivalent plastic strain amplitude. The difference is smaller when the comparison is made in terms of equivalent stress amplitude. It is possible to fit all the endurance results by using the following mechanical loading parameter : $\gamma_{max}/2 + \Delta\epsilon_n/2$, where $\gamma_{max}/2$ is the maximum shear strain amplitude on the plane experiencing the largest shear strain while $\Delta\epsilon_n$ is the tensile strain applied to this plane.

(6) Intergranular cracking is largely promoted by the application of out-of-phase loadings. Although this effect is not fully understood, it might partly account for the reduction in fatigue life associated with this type of loading.

(7) A three-dimensional analysis of the traces of transgranular initiation sites shows that transgranular fatigue microcracking is closely related to the value of the shear strain amplitude undergone by a given plane. On the other hand the orientation of the macrocrack does not obey a simple rule, especially for the out-of-phase loadings. This might be related to dramatic crack closure effects.

ACKNOWLEDGMENTS : This study was supported by the French Ministery of Research (Contract MRES N°86-A-538). Discussions with Dr. J. DHERS from UNIREC are also acknowledged.

References

[1] "Multiaxial Fatigue" A.S.T.M. STP 853 Miller/Brown Editors. August 1985.

[2] Second International Conference on Biaxial/Multiaxial Fagigue. 16-20 Dec.1985. Sheffield University.

[3] Brown, M.W. and Miller, K.J. "Biaxial cyclic deformation of steels". Fat. of Eng. Mat. and Struc. vol.1, 1979, pp.93-106.

[4] Sonsino, C.M. and Grubisic, V. "Fatigue behavior of cyclically softening and hardening steels under multiaxial elastic-plastic deformation". Multiaxial Fatigue A.S.T.M. STP 853, 1985, pp.586-605.

[5] Parsons, M.W. and Pascoe, K.J. "Observations of surface deformation, crack initiation and crack growth in low cycle fatigue under biaxial stress", Mat. Sci. and Eng., vol.22, 1976, pp.31-50.

[6] Socie, D. "Multiaxial fatigue damage models "Journal of Eng. Mat. and Techn., vol.109, Oct.87, pp.293-298.

[7] Kanazawa, K., Miller, K.J. and Brown, M.W. "Cyclic deformation of 1% CrMoV. Steel under out of phase loads", Fat. of Eng. Mat. and Struc., vol.2, 1979, pp.217-228.

[8] Jacquelin, B., Hourlier, F. and Pineau, A. "Crack initiation under low cycle multiaxial fagigue", A.S.T.M. STP 853, Multiaxial Fagigue, 1985, pp.285-31.

[9] Jacquelin, B. "Amorçage des fissures en fatigue oligocyclique sous chargement multiaxial" Thesis, Ecole des Mines, March 4th, 1983.

[10] Brown, M.W. and Miller, K.J. "A theory for fatigue failure under multiaxial stress-strain conditions" Proceedings. INSTN- Mech. Engrs, vol.187, 1973, pp.65-73.

[11] Cailletaud, G., Doquet, V. and Pineau, A. "Prediction of macroscopic multiaxial behaviour from microstructural observations" This volume.

[12] Robillard, M. and Cailletaud, G. "Directionaly defined damage in multiaxial low cycle fatigue : experimental evidence and tentative modelling". This volume.

[13] Williams, R.A., Racek, R.J., Klufas, O., Adams, S. and Gonyea, D.C. "Biaxial torsional fatigue of turbine generator rotor steels" A.S.T.M. STP, 853, Multiaxial Fatigue, 1985, pp.440-462.

[14] Smith, E.W. and Pascoe, K. "Fatigue crack initiation and growth in a high strength ductile steel subject to in-plane biaxial loading", A.S.T.M. STP, 853, Multiaxial Fatigue, 1985, pp.111-134.

[15] Brown, M.W. and Miller, K.J. "Mode I fatigue crack growth under biaxial stress at room and elevated temperature" A.S.T.M. STP, 853, Multiaxial Fatigue, 1985, pp.135-152.

[16] Ritchie, R.O. McClintock, F.A. Tschegg E.K. and Nayeb-Hashemi H. "Mode III fatigue crack growth under combined torsional and axial loading" A.S.T.M. STP 853, Multiaxial Fatigue, 1985, pp.203-227.

[17] Hua, C.T. and Socie, D.F. "Fatigue damage in 1045 steel under constant amplitude biaxial loading" Fat. of Eng. Mat. and Struct., vol.7, 1984, pp.165-179.

[18] Doquet, V. "Amorçage des fissures de fatigue sur tôles minces revêtues" Report Ecole des Mines, January 1989.

[19] Hourlier, F., d'Hondt, H., Truchon, M. and Pineau, A. "Fagigue crack path behavior under polymodal fatigue" A.S.T.M. STP 853, Multiaxial Fatigue, 1985, pp.228-248.

[20] Inoue, T., Hoshide, T., Yoshikawa, T. and Kimura, Y. "Slip band behavior and crack initiation in polycristalline copper under multiaxial low cycle fatigue - a damage mechanics approach", Eng. Fract. Mech., vol.25, n°5/6, 1986, pp;665-675.

[21] Sakane, M., Ohnami, M. and Sawada, M. "Fracture modes and low cycle biaxial fatigue life at elevated temperatures" Journal of Eng. Mat. and Struc., vol.109, 1987, pp.236-243.

C	N	Mn	Ni	Cr	Si	Cu	Al	P	S
49	2	188	20	13	9	13	64	14	17

Table 1 : Chemical composition of mild steel (10^{-3} Weight %).

Upper yield strength (MPa)	Lower yield strength (MPa)	U.T.S. (MPa)	Elongation (%)	E (MPa)	μ (MPa)
263	210	316	37	210000	74800

Table 2 : Mechanical propertis of mild steel.

Test	$\Delta\varepsilon/2$ (%)	$\Delta\varepsilon_p/2$ (%)	$\Delta\sigma/2$ (MPa)	N_f (cycles)
A1	1.0	0.85	319	516(*)
F2	1.0	0.85	308	1010
A3	1.0	0.86	298	1886
C2	0.5	0.38	255	5500
I1	0.494	0.376	246	1522(*)
H1	0.49	0.36	275	4430
A2	0.3	0.19	232	11120
I2	0.249	0.16	185	9359(*)
D1	0.21	0.118	196	19311
B5	0.18	0.1	171	17471(*)
F1	0.149	0.078	149	136405
B3	0.109	0.044	139	124177
307	0.074	0,014	125	289694
D4	0.063	0.009	115	773700

(*) premature failure.

Table 3 : Tension-compression tests carried out under displacement control except. Test 307.

Test	$\Delta\gamma/2$ (%)	$\Delta\gamma_p/2$ (%)	$\Delta\tau/2$ (MPa)	N_f (cycles)
C5	1.59	1.33	159	1079
D6	0.89	0.7	138	3341
A6	0.46	0.31	110	26381
301	0.43	0.295	109	41788
C6	0.27	0.15	92.5	71041
B4	0.158	0.066	65	581328

Table 4 - Reversed torsion tests carried out under displacement control except Test 301.

Test	$\Delta\varepsilon/2$ (%)	$\Delta\gamma/2$ (%)	$\Delta\sigma/2$ (MPa)	$\Delta\tau/2$ (MPa)	Phase angle (degrées)	$\Delta\varepsilon_{eq\,Mises}/2$ (%)	$\Delta\varepsilon_{eq\,Tresca}/2$ (%)	$\Delta\sigma_{eq\,Mises}/2$ (MPa)	$\Delta\sigma_{eq\,Tresca}/2$ (MPa)	N_f (cycles)
234			215	101	0			267	285	3570
306	0.34	0.62	165	107	0			243	264	3381
340c	0.21	0.378	166	77	0	0.305	0.391	210	224	interrupted
340b	0.144	0.247	147	72	0	0.2	0.216	193	205	interrupted
205			136	65	0			177	189	20774
340a	0.077	0.122	137	66.5	0	0.101	0.109	176	186	interrupted
251	0.13	0.29	95	79	0	0.22	0.23	165	185	28417
305	0.1	0.19	102	61	0	0.144	0.162	144	156	114574
233			274	141	90			274	293	2717
232	0.25	0.59	270	144	90	0.33	0.375	270	289	3041
250	0.235	0.43	238	133	90	0.28	0.29	235	255	4610
201	0.13	0.23	219	127	90	0.145	0.157	227	247	15432
253	0.165	0.28	216	118	90	0.18	0.195	218	236	prématurе failure
304	0.1	0.185	144	87	90	0.107	0.12	159	171	50498
252	0.105	0.184	137	83	90	0.126	0.137	152	171	23858
308	0.067	0.105	121	73	90	0.078	0.089	129	146	112850
302	0.096	0.18	150	86	130	0.126	0.135	165	179	89898

Table 5 - Combined tension and torsion tests. Those the number of which is underlined were carried out under displacement control.

Test Number	Loading mode	N_f (Cycles)	Intergranular cracking (%)	Transgranular cracking (%)	undetermined (%)
B5	tension	17471	26	74	0
301	torsion	41788	45	55	0
305	in-phase	114574	35	65	0
251	tension and	28417	45	55	0
234	torsion	3570	42	46	10
201	out-of-phase	15432	68	28	4
250	tension and	4610	81	19	0
233	torsion	2717	71	16	13

Table 6 : Ratio of intergranular and transgranular cracking.

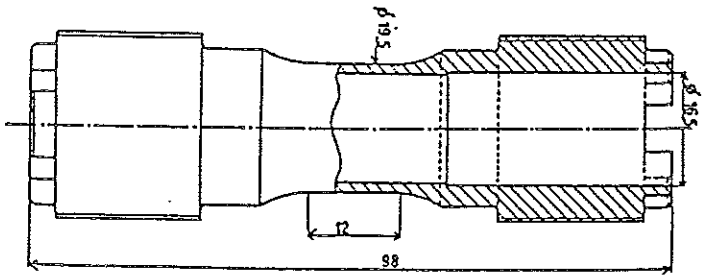

Fig. 1 - Geometry of the specimens.

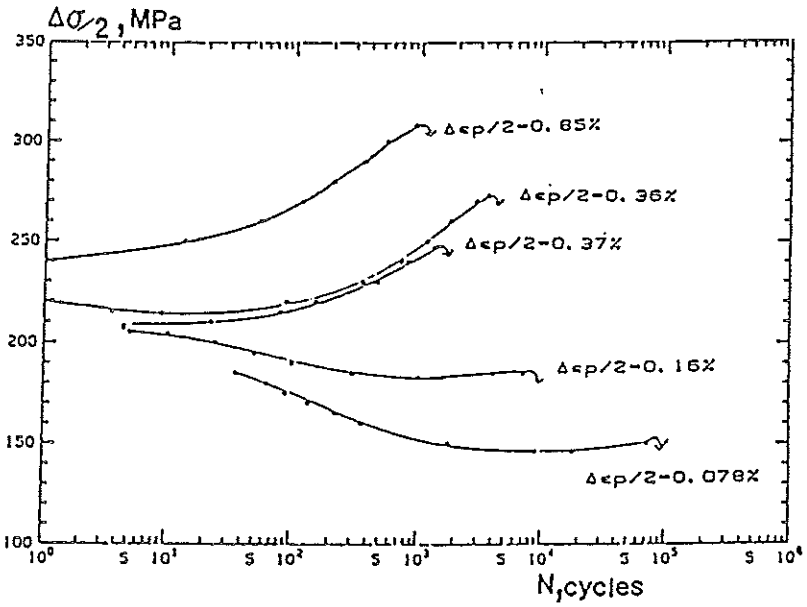

Fig. 2 - Variation of the stress amplitude during tension - compression tests as a function of plastic strain amplitude.

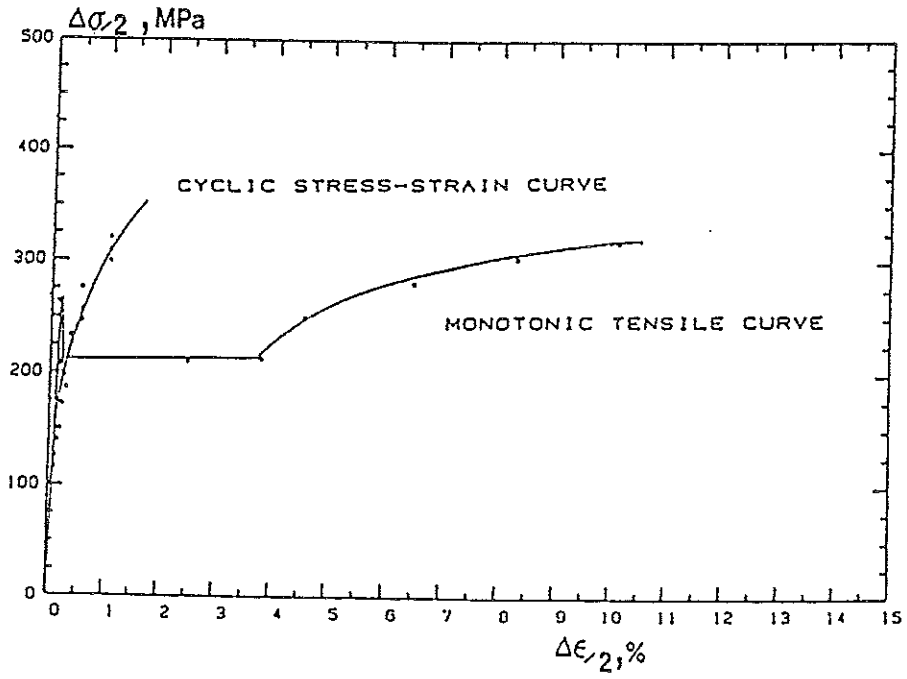

Fig. 3 - Monotonic and cyclic tensile stress-strain curves.

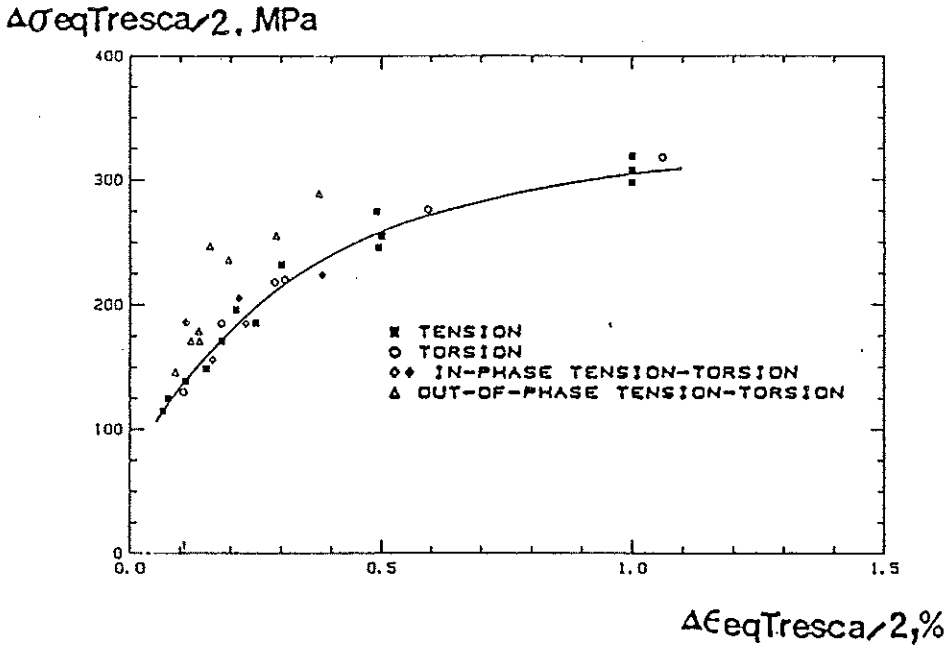

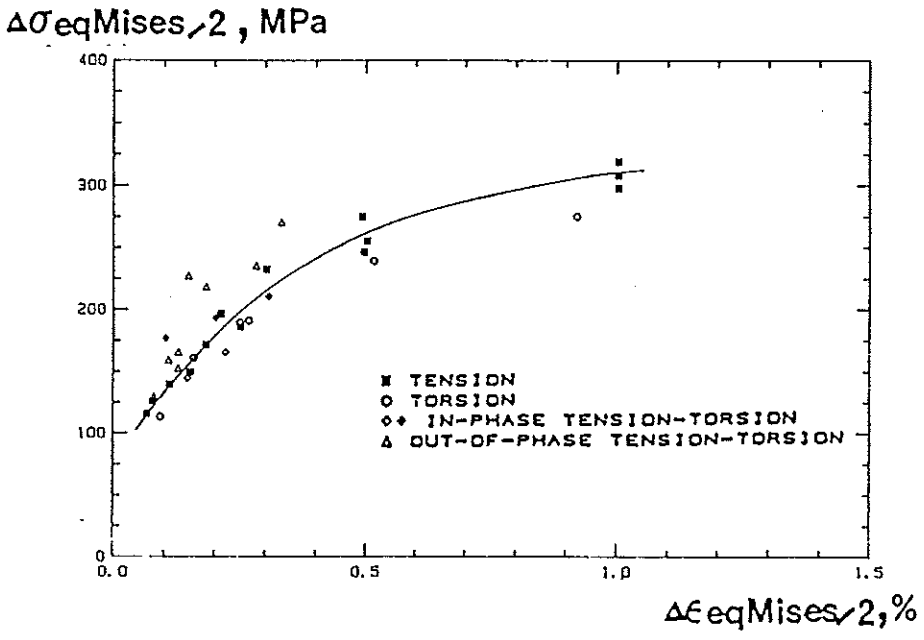

Fig. 4 - Uniaxial and multiaxial stress-strain behaviour using. a) Tresca's; b) Von Mises's équivalents.

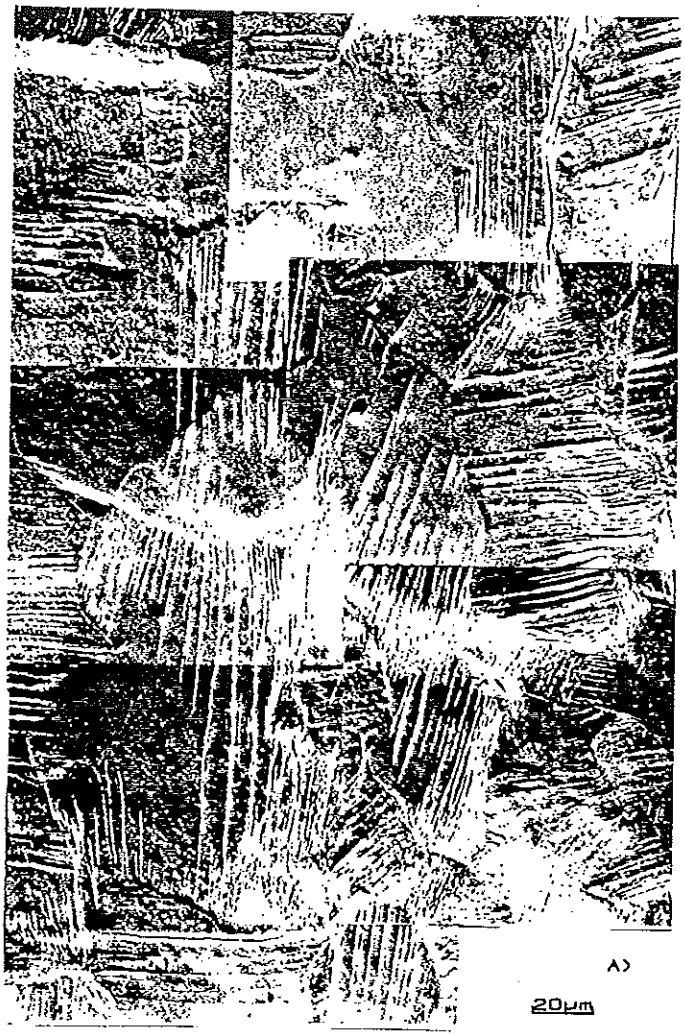

Fig. 5 - Micrographs of the outer surface of specimens subjected to
a) in-phase tension and torsion (test 251);
b) out-of-phase tension and torsion (test 232).

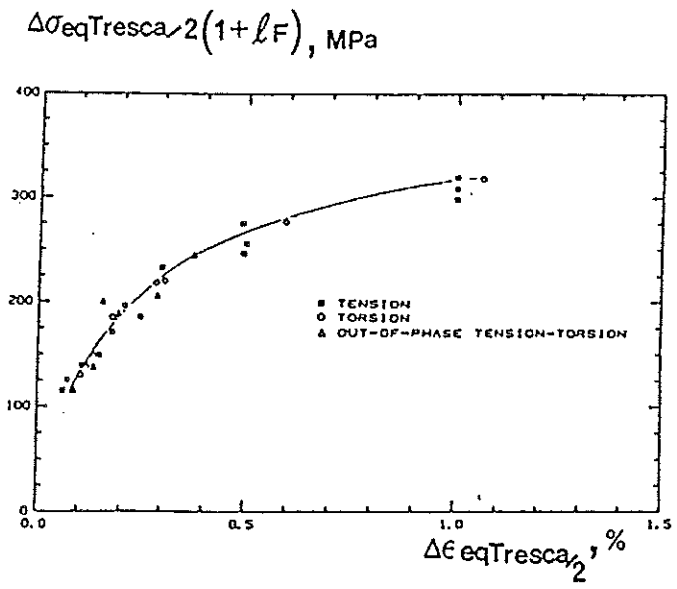

Fig. 6 - Representation of the cyclic behaviour of mild steel with Kanazawa, et al's parameter.

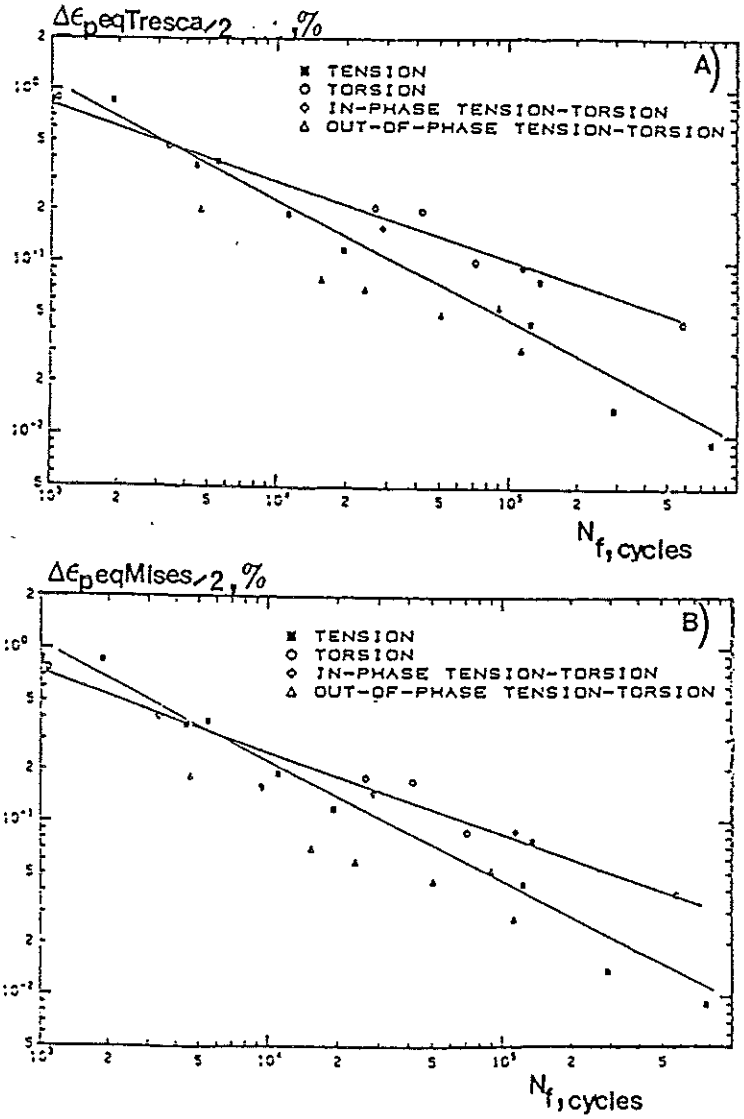

Fig. 7 - Endurance of the specimens drawn versus :

a) Tresca's;

b) Von Mises's equivalent plastic strain amplitude.

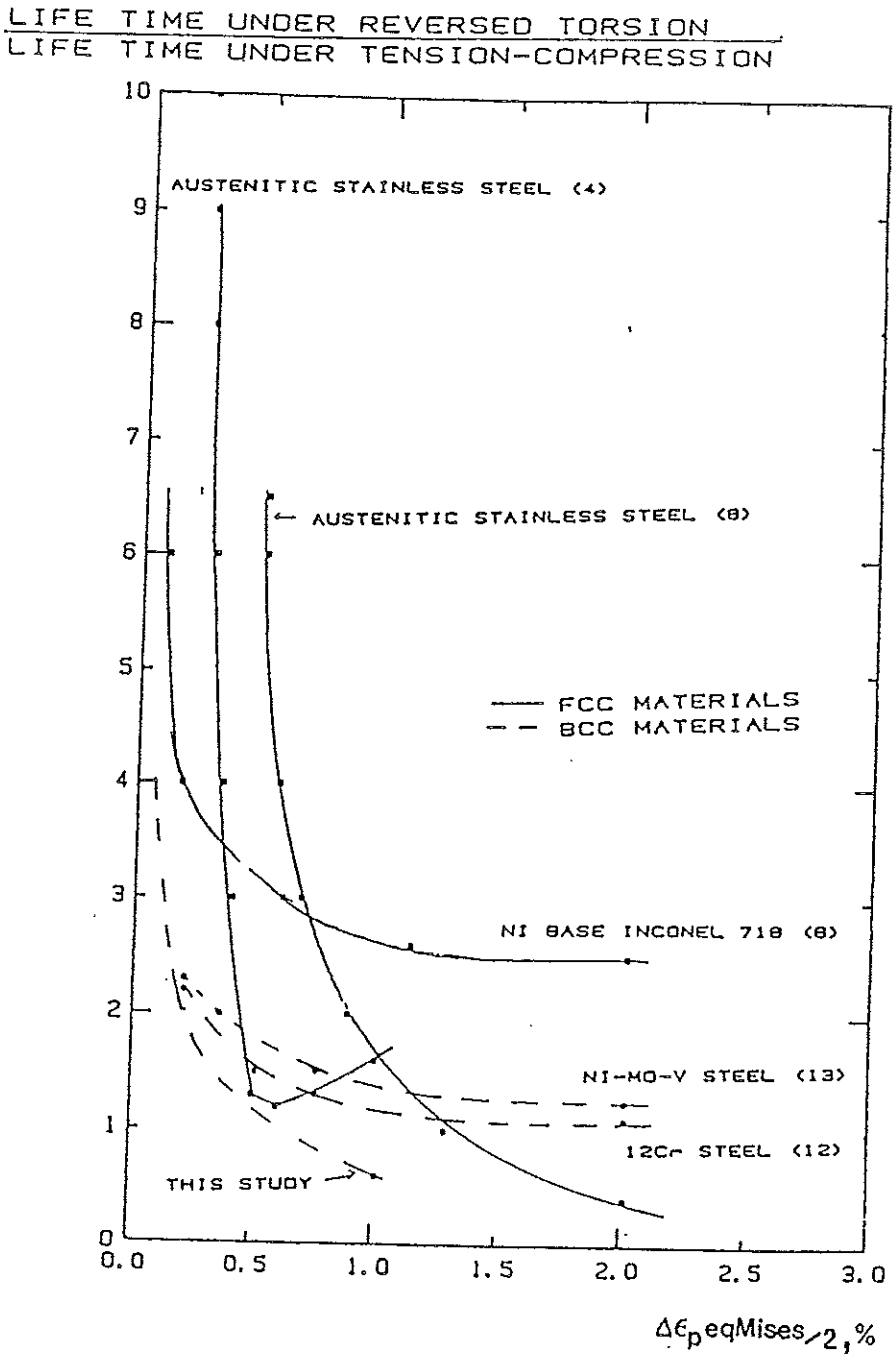

Fig. 8 - Comparison between life-times under tension or torsion for several materials from the literature.

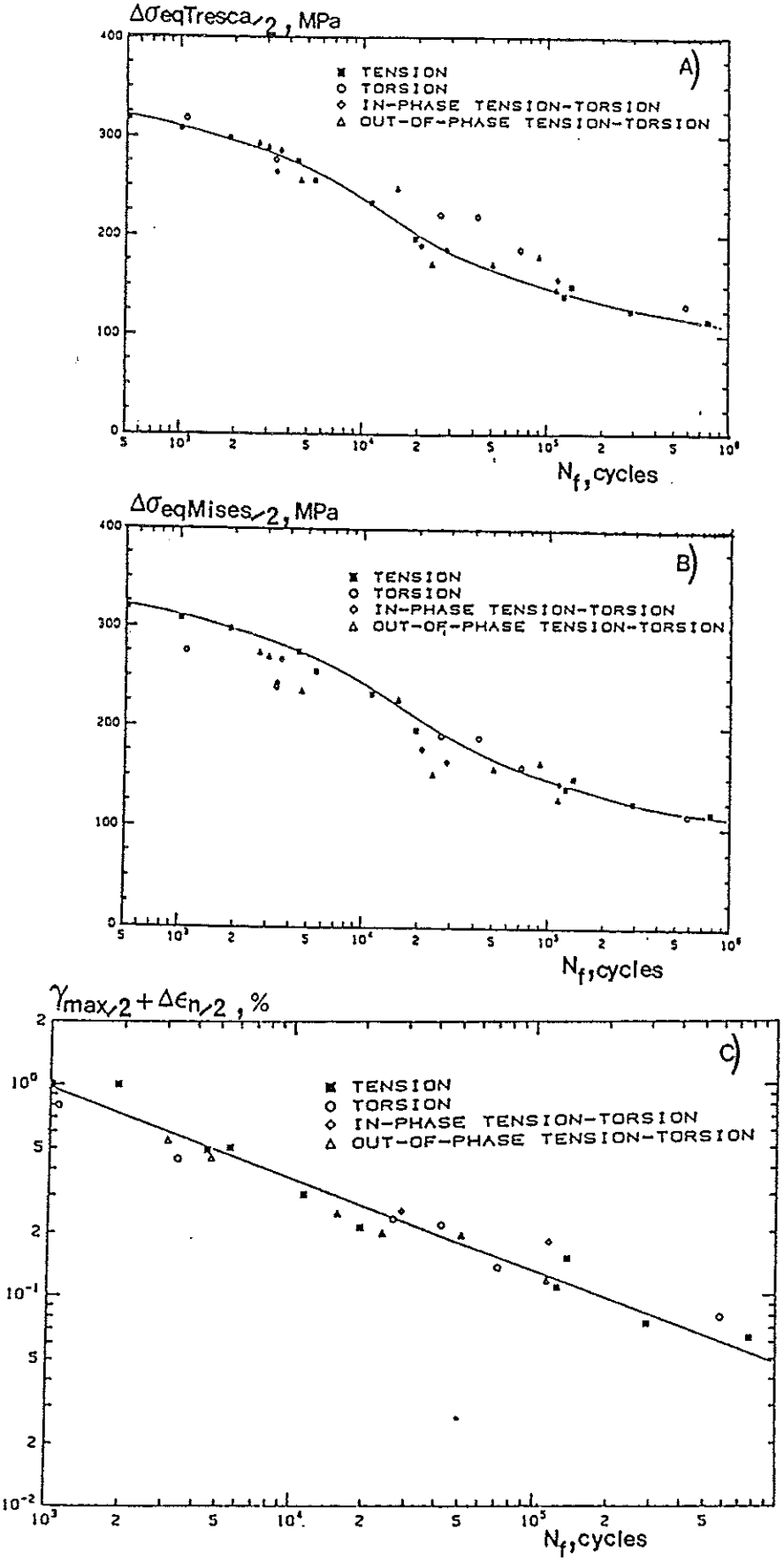

Fig. 9 - Endurance of the specimens drawn versus :
a) Tresca's;
b) Von Mises's equivalent stress amplitude;
c) a parameter derived from Socie's one.

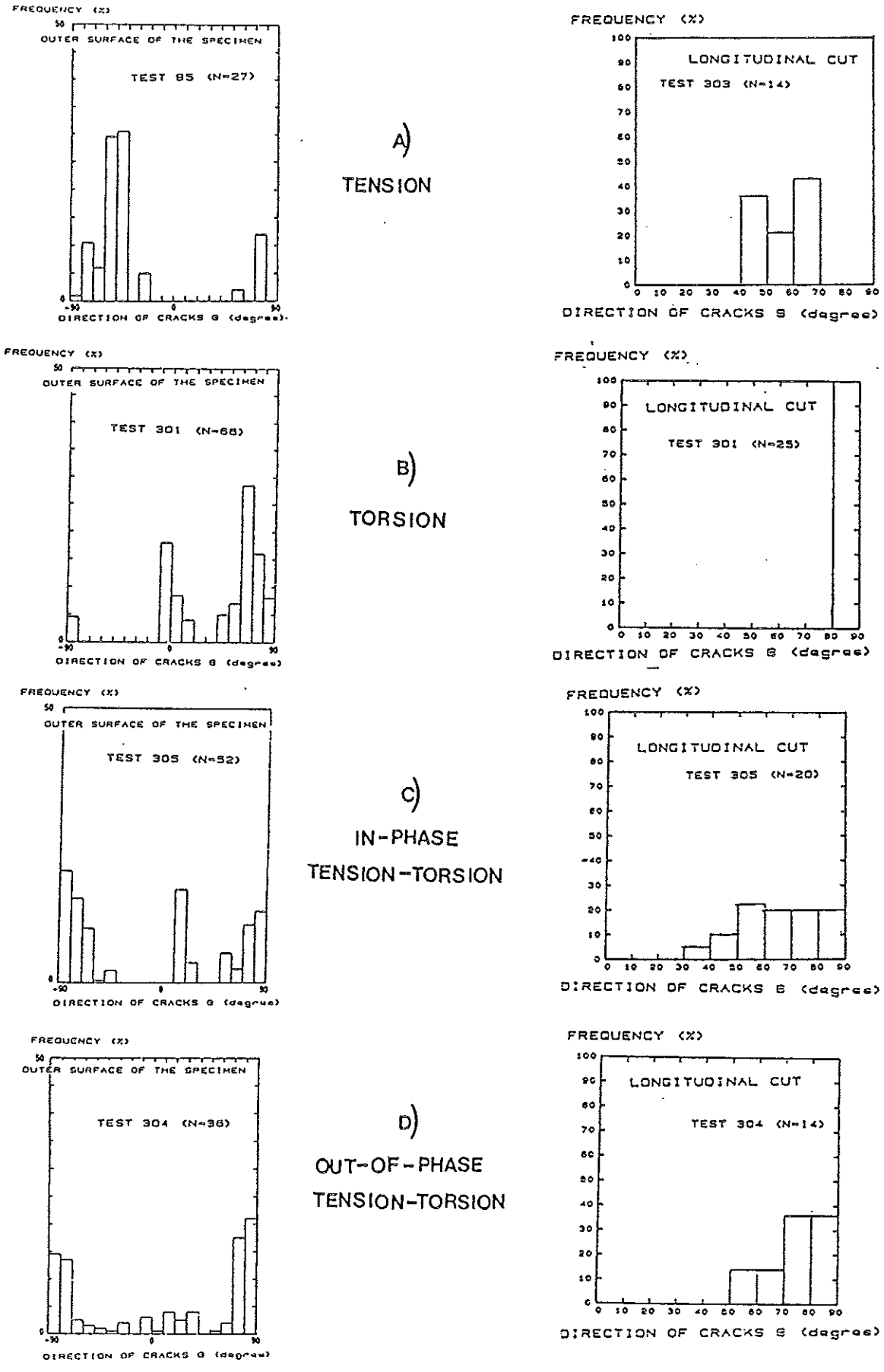

Fig.10 - Histograms showing the angular distribution of damage around the axis of the specimens (N is the number of cracks analyzed).

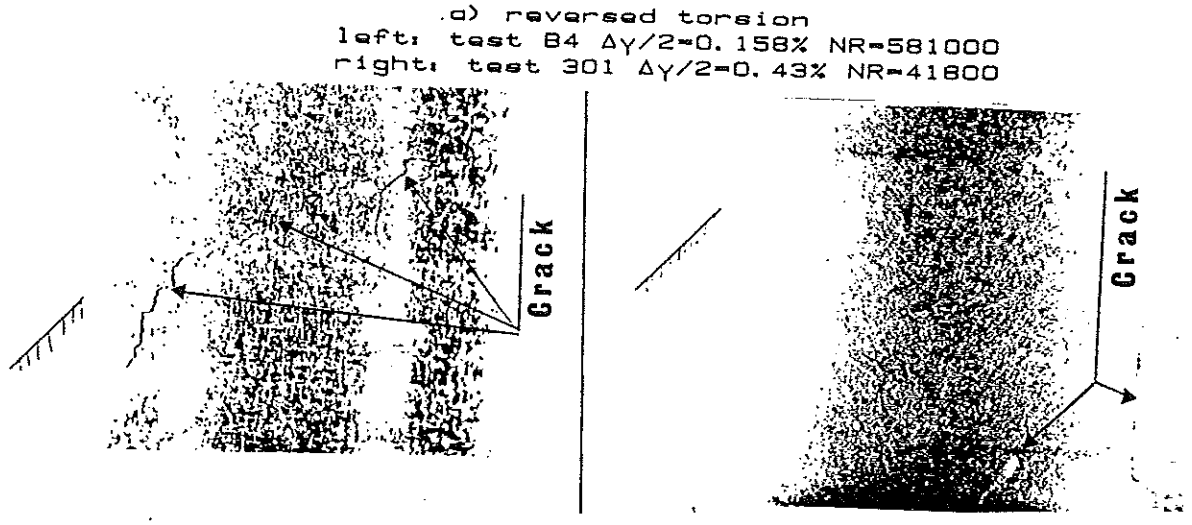

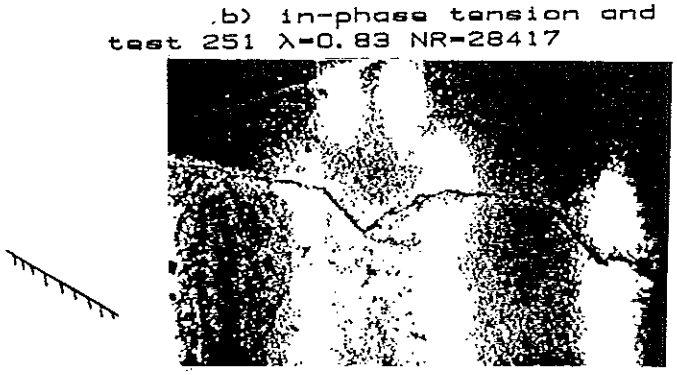

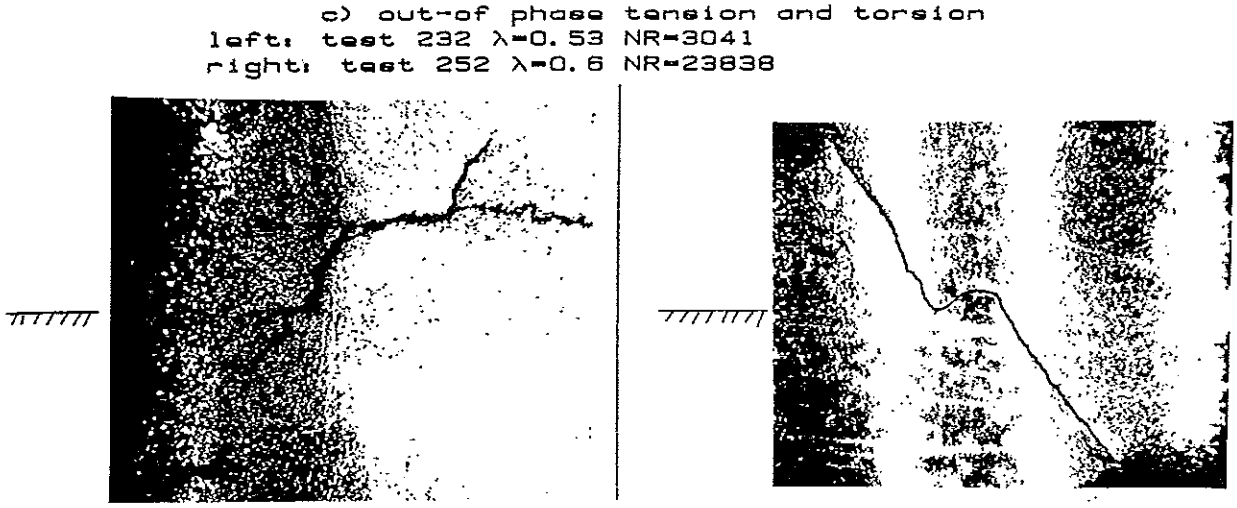

Fig.11 - Directions of main cracks in several specimens compared with directions of planes (drawn) undergoing the largest amplitude of opening stress (average magnification X8. Loading axis is along the vertical axis)